

Document downloaded from:

<http://hdl.handle.net/10251/102167>

This paper must be cited as:



The final publication is available at

<https://doi.org/10.1177/1468087417697759>

Copyright SAGE Publications

Additional Information

---

# Effects of cavitation in common-rail diesel nozzles on the mixing process

Journal Title

XX(X):1–23

©The Author(s) 2015

Reprints and permission:

sagepub.co.uk/journalsPermissions.nav

DOI: 10.1177/ToBeAssigned

www.sagepub.com/



J. Javier López<sup>1</sup>, Oscar A. de la Garza<sup>2</sup>, Joaquin De la Morena<sup>1</sup> and S. Martínez-Martínez<sup>2</sup>

## Abstract

A study to experimentally analyze the effect of cavitation on the mixing process in diesel nozzles was carried out. The mixing process was studied through the spray cone angle. It was characterized in two different scenarios: with the liquid length (nearly realistic conditions, i.e. evaporative but non-reactive spray) and the heat release fraction (fully realistic conditions, i.e. evaporative and reactive spray). In both studied scenarios the increase of spray cone angle caused by the cavitation phenomenon, which leads to a better mixing process, has been confirmed.

Nevertheless, when the variations of the effective injection velocity and the spray cone angle obtained by comparing a cylindrical nozzle (i.e. a nozzle that promotes the cavitation phenomenon) with a conical nozzle (i.e. a nozzle that inhibits this phenomenon) were analyzed together, it was found that, for the cases studied here, the mixing process worsens with the cylindrical nozzle.

## Keywords

Diesel nozzle, cavitation, injection process, spray cone angle, combustion process

## Introduction

Among the ways to fulfil the requirements of customers and the legislations regarding pollutant emissions, the design of the nozzle geometry in a diesel engine is an important factor to improve the combustion process. It might lead to a reduction of the pollutant emissions, as demonstrated by Karra and Kong<sup>1</sup> and Som et al.<sup>2</sup>. These authors showed that the nozzle geometry has a significant impact on soot emissions. This can be explained by the influence of the nozzle geometry on the internal flow and the characteristics of the spray, especially on the atomization and mixing processes. In fact, this is the main reason why many studies, such as: Payri et al.<sup>3</sup>, Wang et al.<sup>4</sup>, Som et al.<sup>2</sup>, Watanabe et

al.<sup>5</sup> and Hayashi et al.<sup>6</sup> have analyzed the effect of the nozzle

---

<sup>1</sup> CMT-Motores Térmicos, Universitat Politècnica de València, Spain  
Camino de Vera, s/n. 46022 Valencia, SPAIN

<sup>2</sup> Universidad Autónoma de Nuevo León-FIME, LIITE-Laboratory for Research and Innovation in Energy Technology

### Corresponding author:

Dr. Oscar A. de la Garza

Universidad Autónoma de Nuevo León-FIME,

LIITE-Laboratory for Research and Innovation in Energy Technology

Av. Universidad s/n. Ciudad Universitaria, San Nicolás de los Garza,

Nuevo León, C.P. 66455, MEXICO

Tlf: +52 81 83 29 4000 ext:1636, Fax: +52 81 83 32 09 04

Email: oscar.delagarzadl@uanl.edu.mx

geometry on the internal flow and the characteristics of the spray.

One of the most significant aspects in this sense is the formation of cavitation inside the nozzle. This cavitation can appear in different zones of the nozzle depending on the flow condition. First, cavitation can be induced due to the flow separation at the nozzle orifices inlet, where the pressure drop can decrease significantly when high flow velocities are reached. Studies by Nurick<sup>7</sup> and Schmidt<sup>8</sup> showed that this cavitation formation depends strongly on the nozzle geometry, and in particular they observed that this kind of cavitation can be avoided by combining high conicity in the nozzle orifices and high hydrogrinding rates (which result in high rounding radii at the orifices inlet). The formation of this cavitation has shown to significantly affect the nozzle permeability characteristics, due to a significant decrease in the nozzle effective diameter<sup>9</sup>. Gavaises et al.<sup>10</sup> detected that string cavitation can also appear in diesel injector nozzles. This string cavitation is induced by a vortex flow created at the inlet of the nozzle orifices, and can appear both in VCO<sup>11</sup> or sac nozzles<sup>12</sup>, although they tend to reduce as the sac volume increases. Finally, cavitation can also appear in the needle seat area when the needle is placed at low lift conditions<sup>13;14</sup>

Visualization techniques have been applied on transparent nozzles to better understand the characteristics of the cavitating flow. Soteriou et al.<sup>15</sup> saw that the cavitation region was formed as a cloud of small bubbles. Studies on real-scale geometries by Chaves et al.<sup>16</sup> and Arcoumanis et al.<sup>17</sup> detected cavitation as a set of film structures. Winklhofer et al.<sup>18</sup> and Payri et al.<sup>19;20</sup> showed that the onset of cavitation appears for cavitation number conditions lower than the mass flow collapse. Additionally, Winklhofer et al. measured an increase in the flow velocity near the interphase between liquid and vapor, which is consistent with the increase in effective outlet velocity observed through momentum flux measurements at the nozzle outlet<sup>21</sup>. Mishra

and Peles<sup>22</sup> detected a hysteresis phenomena associated with the onset of cavitation. Aleifeiris et al.<sup>23</sup> and Jiang et al.<sup>24</sup> confirmed the influence of the fluid properties (mostly density and viscosity) on the cavitation formation. Sou and Pratama<sup>25</sup> found out that the appearance of cavitation was also affected by the asymmetry of the nozzle layout, since it changes the extent of the recirculation area. Recently, x-ray visualization techniques have been applied to characterize cavitation formation in metal nozzles, arriving to similar conclusions than the previous studies<sup>26</sup>.

In parallel to the experimental studies previously summarized, different numerical methodologies have been developed to study the details of cavitating flows. While some models predicted cavitation by means of bubbles growth based on Rayleigh-Plesset equation<sup>27-29</sup>, homogeneous mixture approaches are generally accepted as the most suitable for diesel nozzle modeling<sup>8;30;31</sup>. Such models, once validated, have been used to evaluate the influence of certain characteristics of the nozzle and injector geometry on cavitation formation, such as the orifice inclination angle<sup>32</sup>, the orifice conicity<sup>33;34</sup>, the orifice shape<sup>35</sup> or the off-axis needle motion<sup>36</sup>. Lately, numerical approaches trying to combine the simulation of cavitation inside the nozzle and the spray formation are being developed<sup>37</sup>.

The appearance of cavitation inside the nozzle has an impact not only on the injector hydraulic behavior, but also on the spray formation. In particular, cavitation has shown to act as an enhancer of the fuel atomization<sup>15;38</sup>. Regarding the mixing process, Chaves et al.<sup>16</sup> studied the spray cone angle in non-reactive and non-evaporative conditions. Under supercavitation conditions, these authors observed an increase in the spray cone angle, which lead to a better mixing process. Other authors, such as Payri et al.<sup>39</sup>, Andriotis et al.<sup>40</sup> and Boggavarapu et al.<sup>41</sup> also related the cavitating flow with an increase in the spray angle at ambient temperature conditions. Similar findings have been

found for sprays injected at high temperature but on an inert environment<sup>42;43</sup>. Finally, Payri et al.<sup>42</sup> and Benajes et al.<sup>44</sup> studied the spray cone angle but now in fully realistic conditions (i.e. evaporative and reactive spray): in the first case, the increase of the spray cone angle as a consequence of the cavitation phenomenon was confirmed, while in the second case the opposite trend was found: a lower spray cone angle under cavitating conditions, which lead to a worse mixing process. These last two studies show that the possible potential of a cylindrical nozzle (i.e. cavitating nozzle) on the mixing process is not yet clear. For this reason, the objective of the present publication is to go further in the knowledge of the effect of cavitation on the mixing process in diesel nozzles.

In order to reach the objective previously described, the present article is divided in four additional sections, the contents of which will be presented now: in section “Experimental equipment”, the experimental tools that will be employed in the study will be presented. The experimental and analysis methodology will be described in section “Experimental and analysis methodology”. In section “Results and discussion”, the results obtained about the effect of cavitation on the effective nozzle diameter, the effective injection velocity and the spray cone angle will be presented and discussed. And finally, the more relevant conclusions of the study will be summarized in the “Conclusions” section.

## Experimental equipment

### Nozzles

Two three-hole nozzles were used in the study, which were mounted in a piezo-electric injector holder. One of the nozzles inhibits the cavitation phenomenon (a conical nozzle with high level of hydro-grinding), whereas the other one promotes the appearance of the cavitation phenomenon (cylindrical nozzle without hydro-grinding). Both nozzles

have a different conicity level. This level is quantified by the k-factor, which is defined in the following way:

$$k - factor = \frac{d_{in} - d_{out}}{10} \quad (1)$$

where  $d_{out}$  is the nozzle outlet diameter and  $d_{in}$  is the nozzle inlet diameter, both in  $\mu m$ . In Table 1 the geometrical details, which were obtained through the silicone methodology<sup>45</sup>, are given.

**Table 1.** Geometrical details of the nozzles used in the study.

Nozzle	$d_{in}$ [ $\mu m$ ]	$d_{out}$ [ $\mu m$ ]	k-factor [-]
Conical nozzle	135	105	3
Cylindrical nozzle	122	122	0

### Mass Flow Rate Meter

The measurement of the instantaneous mass flow rate was carried out in a dedicated test rig<sup>46</sup>, which is based on the Bosch or long tube method. In this device, the pressure increase induced by the injection process is registered and post-processed to extract the information about the mass flow rate. Further details of this method are available in references<sup>47</sup> and<sup>48</sup>.

### Momentum Flux Test Rig

The measurement of momentum flux was carried out in a dedicated test rig. The momentum flux was measured when the spray impacted a target attached to a piezoelectric pressure sensor localized at a distance of 5 mm of the nozzle hole<sup>47</sup>. The impact area is sufficiently large to ensure that all the spray impacts on this area. More details of this experimental equipment are available in<sup>47</sup>.

### Optically Accessible Engine

The optically-accessible engine is a two stroke, single-cylinder engine equipped with a cylinder head including a combustion chamber with an optical access. The technical data of this engine are given in Table 2. This experimental facility can work in two different configurations: reacting

and non-reacting. In the reacting configuration, air is used as working fluid, and this configuration is used to characterize the combustion process. In the non-reactive, evaporative configuration, nitrogen is used as working fluid, and this other configuration is the one used to characterize the mixing process. More details about this experimental facility are available in<sup>49</sup>.

**Table 2.** Technical characteristics of the optically-accessible engine.

Bore	150 mm
Stroke	170 mm
Effective stroke	108 mm
Compression Ratio	22.5:1
Rotational speed	500 r.p.m
Total engine displacement	3000 cm <sup>3</sup>

### Direct illumination by Mie-Scattering

This optical technique is based on obtaining images of a diesel spray illuminated in a direct way by a light beam generated thanks to a continuous light source. More details of the optical setup that has been used to apply this optical technique are available in<sup>50</sup>.

### Single-Cylinder Engine

The single-cylinder engine is representative of a small automotive engine for passenger cars: it is derived from the DV6-TED4 engine from PSA Peugeot-Citroën, with four valves per cylinder. The main characteristics of this single-cylinder engine are given in Table 3.

**Table 3.** Main technical characteristics of the single-cylinder engine DV6-TED4.

Bore	75.1 mm
Stroke	88.0 mm
Displacement volume	399 cm <sup>3</sup>
Connecting rod length	123.8 mm
Bowl diameter	46.3 mm
Depth of bowl	14.3 mm
Compression ratio	16.5
Exhaust valve diameter	23.4 mm
Intake valve diameter	25.6 mm
Swirl number	2.15
Bowl volume	18.3 cm <sup>3</sup>
Number of valves per cylinder	4

### Test Fuel

Finally, all experiments were carried out with a standard diesel fuel, with a density (according to the EN ISO 12185/96 standards at 15 °C) of 842.1 kg/m<sup>3</sup>, and a kinematic viscosity (according to EN ISO 3104/99 standards at 40 °C) of 2.820 · 10<sup>-6</sup> m<sup>2</sup>/s.

## Experimental and analysis methodology

### Hydraulic characterization

In this section, on the one hand, the aspects related to the measurement of the mass flow rate and the momentum flux will be described. On the other hand, the characteristic flow parameters, which are determined with the experimental measurements previously described, will be presented.

#### Measurement of the mass flow rate

A mass flow meter was used to measure the mass flow rate. The measurement was carried out for long injection durations (an electric pulse of 4 ms has been used) to get a stable average value for this parameter. In Figure 1, an example of a measurement of mass flow rate, carried out with the conical nozzle, is shown. In the figure, the range (black ellipse) that has been considered to get an average value of mass flow rate is also shown.

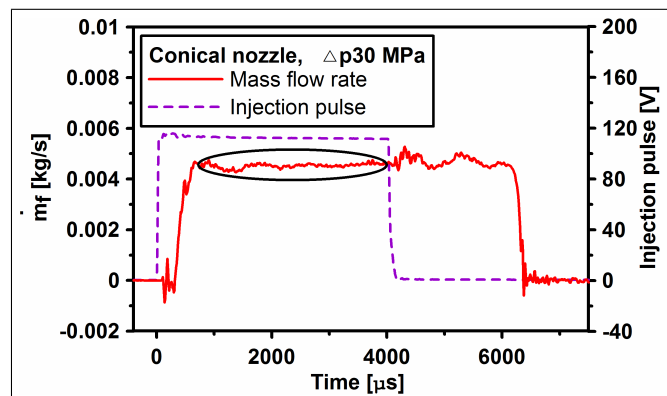


**Figure 1.** Example of a measurement of mass flow rate.

For both nozzles, the measurements were carried out at three different levels of rail pressure ( $p_{rail}$  of 36, 76 and 146 MPa) and a single value of back pressure ( $p_{back}$  of

6 MPa). These operating conditions are representative of those existing in current diesel engines.

### Measurement of momentum flux

A momentum flux test rig was used to measure this other parameter. In a similar way than for the mass flow rate, the measurement was carried out for long injection durations (an electric pulse of 4 ms has been used) to get a stable average value for this parameter. In Figure 2, an example of a measurement of momentum flux, carried out with the conical nozzle, is shown. In the figure the range (black ellipse) that has been considered to get an average value of momentum flux, is also shown.

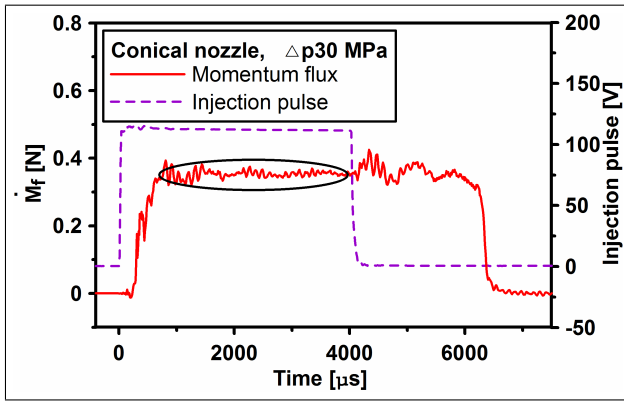


**Figure 2.** Example of a measurement of momentum flux.

In both nozzles, the measurements were carried out in the same operating conditions than for the mass flow rate to get some characteristic flow parameters that will be presented in the next section.

### Characteristic flow parameters

The measurements of mass flow rate and momentum flux described previously are very useful to get some parameters that characterize the flow behavior of nozzles<sup>47</sup>: discharge coefficient,  $C_d$ , momentum coefficient,  $C_M$ , area coefficient,  $C_a$ , and velocity coefficient,  $C_v$ . The latter one characterizes the effective injection velocity and will be used to analyze the spray cone angle calculated either from the liquid length or the heat release fraction. This is the main reason why, in the next lines, more details about the velocity coefficient will be given. However, further details about the other characteristic flow parameters are available in<sup>47</sup>.

The  $C_v$  is defined in the next way:

$$C_v = \frac{u_{eff}}{u_{th}} \quad (2)$$

where  $u_{eff}$  is the effective injection velocity and  $u_{th}$  is the theoretical velocity, which are defined in the following way:

$$u_{eff} = \frac{\dot{M}_f}{\dot{m}_f} \quad \text{and} \quad u_{th} = \sqrt{\frac{2(p_{rail} - p_{back})}{\rho_f}} \quad (3)$$

where  $\dot{M}_f$  is the momentum flux,  $\dot{m}_f$  is the mass flow rate, and  $\rho_f$  is the fuel density. In addition the effective area,  $A_{eff}$ , can be obtained from the experimental measurements described previously. This one is an important parameter to analyze the injection and combustion processes, as already mentioned in the ‘‘Introduction’’ section. In the next lines more details about how it can be obtained will be given. On the one hand, the functional dependence of the mass flow rate is defined by Equation 4:

$$\dot{m}_f = \rho_f \cdot A_{eff} \cdot u_{eff} \quad (4)$$

On the other hand, the functional dependence of the momentum flux is defined by Equation 5:

$$\dot{M}_f = \rho_f \cdot A_{eff} \cdot u_{eff}^2 \quad (5)$$

The combination of Equations 4 and 5 leads to Equation 6, which was described previously:

$$u_{eff} = \frac{\dot{M}_f}{\dot{m}_f} \quad (6)$$

$A_{eff}$  is obtained by relating Equations 5 and 6 in the following way:

$$A_{eff} = \frac{\dot{m}_f^2}{\dot{M}_f \cdot \rho_f} \quad (7)$$

Finally, the effective diameter,  $d_{eff}$ , is obtained from Equation 7, which is defined in the next way:

$$d_{eff} = \sqrt{\frac{\dot{m}_f^2 \cdot 4}{\rho_f \cdot \dot{M}_f \cdot \pi}} \quad (8)$$

### Characterization of the spray cone angle

The spray cone angle is a parameter that characterizes the mixing process, as already mentioned in the ‘‘Introduction’’ section. It will be studied in two different scenarios: based on the liquid length (nearly realistic conditions, i.e. non-reactive evaporative spray) and based on the heat release fraction (fully realistic conditions, i.e. evaporative and reactive spray). In the first scenario two spray cone angles will be analyzed: on the one hand, the one obtained through the functional dependence of the liquid length and, on the other hand, the one measured directly from the images of the liquid phase. In the second scenario, however, only the spray cone angle obtained from the functional dependence of the spray burning rate (assumed to be equivalent to the spray mixing rate) will be used.

#### Characterization of the spray cone angle from experiments of liquid length

The Optically Accessible Engine and the direct illumination by Mie-Scattering technique were used to measure the liquid length. The image acquisition through illumination by Mie-Scattering is composed by a Xenon light source and two optical fibers that lead a light beam until the optical access,

as already mentioned in the ‘‘direct illumination by Mie-Scattering’’ section. The operating conditions, as well as the point of injection, were the same in all the experiments carried out. Regarding the point of injection, it was at TDC, where the thermodynamic conditions are more stable, and at this point the in-cylinder temperature and density were 982 K and 21 kg/m<sup>3</sup>, respectively. Regarding the pressures, they were 36, 76, and 146 MPa for  $p_{rail}$  and 6 MPa for  $p_{back}$ . In addition, in some cases the  $p_{rail}$  level of 26 MPa was added.

The visualization of the liquid length was centered in one of the three nozzle orifices. In Figure 3, to the right, a sample image of liquid length is shown. The color scale of this image is arbitrary, and was selected with the only purpose of better show the liquid length. The spray contour detected by the algorithm developed by Pastor et al.<sup>51</sup> has been added to the image of liquid length, and the value of this parameter in mm is also shown in the image. And in Figure 3, to the left, the position along the engine cycle of the events the most relevant for the corresponding test are shown (i.e. cylinder pressure, injection pulse and mass flow rate). In addition, a black, vertical line has been added to indicate the instant where the liquid length image was obtained. This image corresponds to the cylindrical nozzle, with a  $\Delta p = 30$  MPa ( $p_{rail} = 36$  MPa -  $p_{back} = 6$  MPa).

From the spray contour displayed before, the spray penetration,  $s$ , or liquid length, and the spray cone angle are measured. These two spray parameters are schematically shown in Figure 4. The spray cone angle was obtained through the least-squares fit of two straight lines from the points of the spray contour detected closer to the spray origin. For this fit, five different criteria were considered, taking into account all the points available at 15, 30, 45, 60 and 75% of the spray penetration, thus giving rise to five different values for the spray cone angle. On the one hand, the criterion of 15% of the spray penetration has too few points of the spray contour, and therefore, the statistic fit of the two straight lines

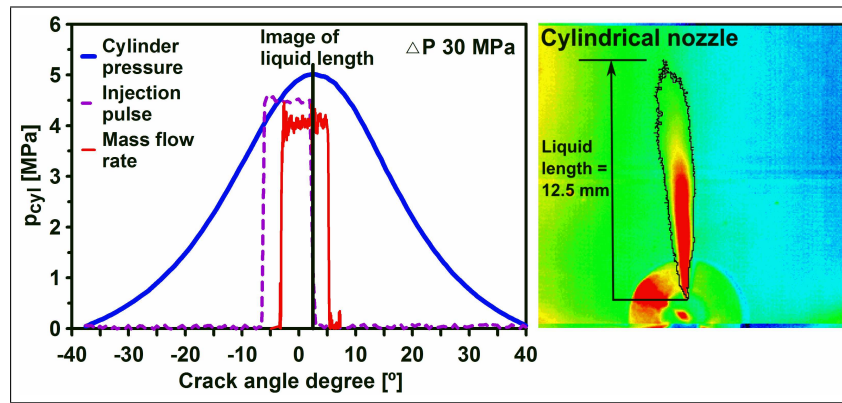


**Figure 3.** Left.- Position in the engine cycle of the events the most relevant for the experiment. Right.- Image of liquid length obtained with the cylindrical nozzle, and with a  $\Delta p = 30 \text{ MPa}$  ( $p_{rail} = 36 \text{ MPa} - p_{back} = 6 \text{ MPa}$ ).

will be little consistent. On the other hand, at the criterion of 75% of the spray penetration, the fitting of the two straight lines is carried out with almost all the points conforming the liquid spray contour, also including those already out of the conical part of the spray. For this reason the corresponding spray cone angle will not be representative of the spray cone angle object of study. Therefore, only the cases: 30, 45 and 60% will be considered in the forthcoming analysis.

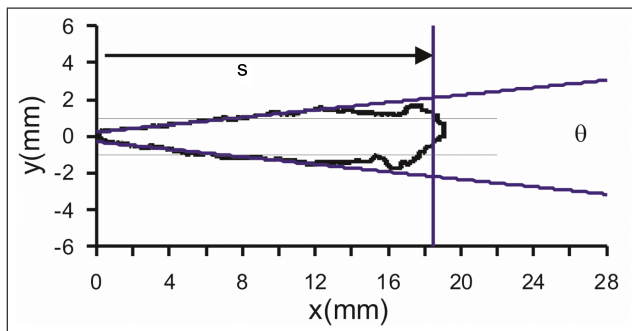


**Figure 4.** Representation of the parameters measured with the image processing algorithm (adapted from García<sup>52</sup>).

Now, the two spray cone angles deduced from these experiments will be presented and discussed.

*Spray cone angle obtained applying the functional dependence of the liquid length*

The first spray cone angle will be obtained like mentioned previously: through the functional dependence of the liquid length. In Figure 5 the temporal evolution of the liquid length during an injection event is shown. In this figure also a region is presented delimited by two vertical dashed lines, which

will be used to obtain an average value of the liquid length that will be employed to analyze the results.

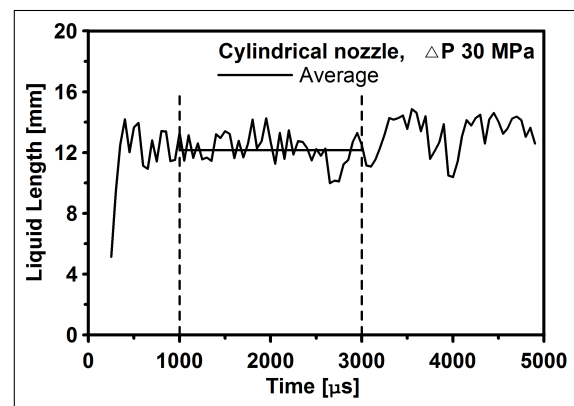


**Figure 5.** Temporal evolution of the liquid length during an injection event.

In Figure 6 the average values of the liquid length for each of the nozzles and  $p_{rail}$  levels studied (36, 76, and 146 MPa) are plotted versus  $p_{rail}$ . In addition, in the figure the confidence interval is shown, taken as  $\pm\sigma$ , where  $\sigma$  is the standard deviation.

Based on the confidence intervals shown in Figure 6, it can be observed that the variation of the liquid length caused by the experimental dispersion is very similar in both nozzles, and is around  $\pm 5\%$ . From the figure, it can be also observed that the injection pressure has no significant effect on the liquid length, which is consistent with the bibliography<sup>53</sup>.

The functional dependence of the liquid length, which will be used to extract information about the spray cone angle, is the following<sup>54</sup>:

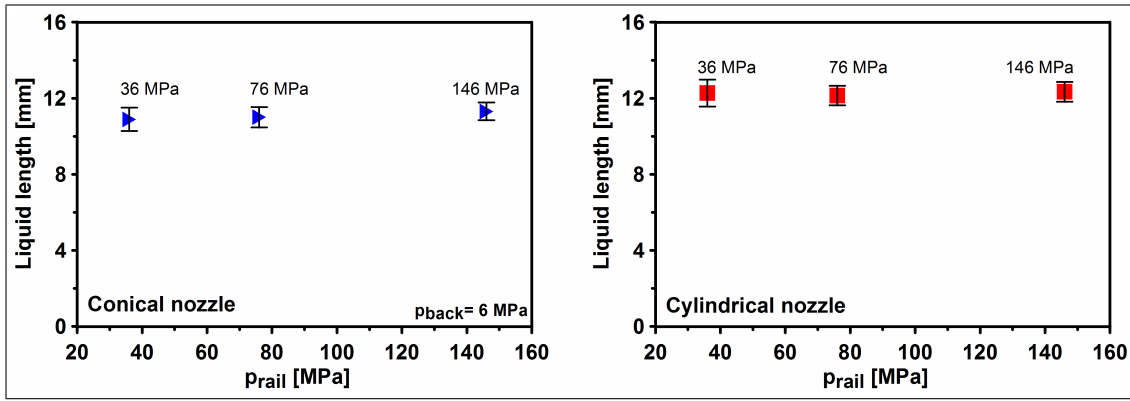


**Figure 6.** Evolution of the liquid length versus  $p_{rail}$ . **Left.**-Conical nozzle. **Right.**- Cylindrical nozzle.

$$LL \propto \frac{d_{eff} \cdot \sqrt{\rho_f / \rho_a}}{Y_{f,evap} \cdot \tan(\theta/2)} \quad (9)$$

where  $d_{eff}$  is the effective diameter, presented previously, and  $Y_{f,evap}$  is the mass fraction of total evaporation of the fuel. This last parameter indicates when the amount of air entrained by the spray is sufficient to completely evaporate the fuel. It depends only on the thermodynamic conditions of the air and the properties of the fuel. The angle obtained from Equation 9 (i.e. the functional dependence of the liquid length) will be referred as  $Ang_{LL.F}$ .

In Figure 7, the average values of  $Ang_{LL.F}$  for each of the nozzles and  $p_{rail}$  levels studied (36, 76, and 146 MPa) are shown. In addition, as in the previous figure, the confidence intervals are also shown, taken as  $\pm\sigma$ , where  $\sigma$  is the standard deviation.

From Figure 7 two aspects can be observed: on the one hand, that the spray cone angle ( $Ang_{LL.F}$ ) decreases as  $p_{rail}$  increases. And, on the other hand, that once  $p_{rail}$  is high enough (e.g. 76 MPa and 146 MPa), the  $p_{rail}$  level do not affect in a significant way the spray cone angle. Both observations are in agreement with the bibliography<sup>55-57</sup>.

Finally it is worthy to note that the authors are aware that the spray cone angle obtained from the liquid length (evaporative but non-reacting spray) is surely different to the spray cone angle that will be obtained later in this paper from the heat release fraction (evaporative and reacting spray).

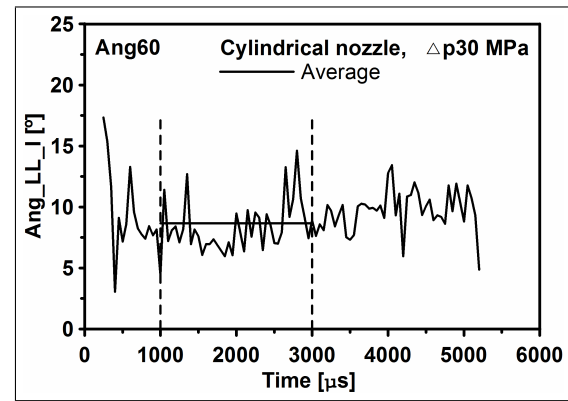


**Figure 8.** Evolution of  $Ang_{LL.I}$  (considering only the spray contour up to 60% of the spray tip penetration) during an injection event.

However these two spray cone angles should be proportional to each other. In fact this will be confirmed by the results that will be presented in the forthcoming subsections.

*Spray cone angle obtained through direct measurement from the images of liquid phase*

The second spray cone angle will be obtained, as mentioned previously, through a direct measurement from the images of liquid phase. This other angle will be referred as  $Ang_{LL.I}$ . In Figure 8 the temporal evolution of  $Ang_{LL.I}$  during an injection event obtained considering only the spray contour up to 60% of the spray tip penetration is shown. In addition, in this figure also a region is presented delimited by two vertical dashed lines, which will be used to obtain an average value of the spray cone angle that will be employed to analyze the results.

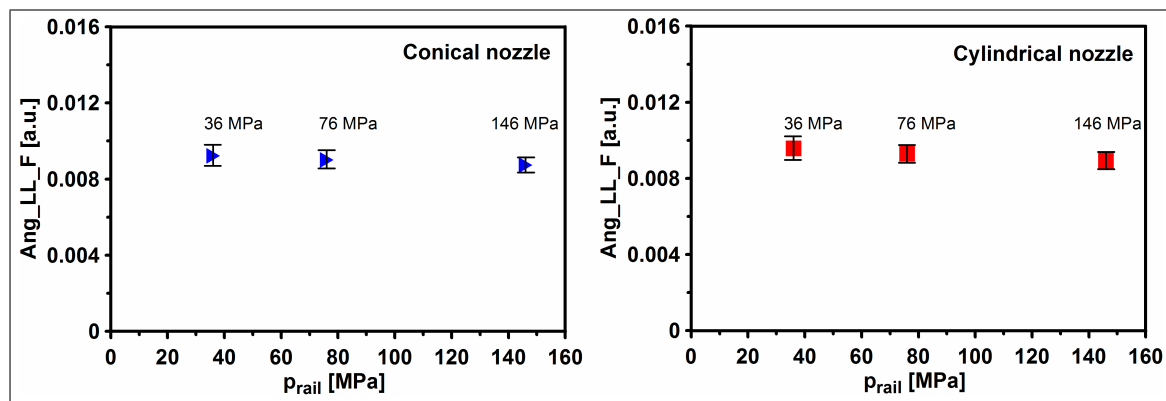


**Figure 7.** Evolution of Ang\_LL.F versus  $p_{rail}$ . **Left.-**Conical nozzle. **Right.-** Cylindrical nozzle.

In Figure 9 the average values of Ang\_LL.I for each of the nozzles and  $p_{rail}$  levels studied (26, 36, 76, and 146 MPa) are plotted versus  $p_{rail}$ . In this figure the confidence interval is also shown. In addition, in this figure the average values from the repetition cases (used for validation purposes) are shown: for the conical nozzle, it corresponds to  $p_{rail}$  36 MPa, while for the cylindrical nozzle it corresponds to  $p_{rail}$  26 MPa. It is worthy to note that, when a sweep of  $p_{rail}$  was completed for a particular nozzle, the first pressure level was tested again with the objective of finding out, on the one hand, the proper operation of the Optically Accessible Engine and, on the other hand, the proper functioning of the high speed camera. These repetitions indicate that both systems/equipments (the engine and the visualization system) have properly operated during the tests for both nozzles.

In Figure 9, if the attention is focused on the results obtained by application of the criterion Ang60 and for the conical nozzle, it can be seen that  $p_{rail}$  does not affect the spray cone angle, which is in agreement with the bibliography<sup>55-57</sup>. In this figure it can also be seen that the repetition case is very coherent for criterion Ang60, or at least more coherent than for the other criteria (Ang30 and Ang45). For these two reasons, the forthcoming analysis will be focused on the results from criterion Ang60 (consequently, further on, Ang\_LL.I will be Ang60). In addition, the spray cone angle at 26 MPa of  $p_{rail}$  for the

conical nozzle has been extrapolated from the three other pressure levels tested, with the objective of allowing the comparison with the corresponding angle of the cylindrical nozzle at this pressure level, since for this other nozzle this pressure was included in the testing plan.

In the next section more details about the second scenario that will be employed to characterize the spray cone angle (i.e. the heat release fraction) will be given.

#### *Characterization of the spray cone angle from experiments of heat release fraction*

The heat release fraction (HRF) is related to the thermal energy released during the combustion process, and is a function of the crank angle. This parameter is determined through an in-house combustion diagnostic model called CALMEC<sup>58,59</sup>, developed at CMT-Motores Térmicos. It is a zero dimensional, sigle zone model, which is based, on the one hand, on the resolution of first principle of Thermodynamics for an open system and, on the other hand, on the equation of state. One of the main hypotheses assumed in this model, for simplicity reasons, is that both the pressure and temperature are uniform inside the cylinder.

The combustion diagnostic model needs several data to operate, such as: the instantaneous in-cylinder pressure signal, geometrical data of the engine (bore, stroke...) and of its operation (engine speed, fuel mass flow rate...) and, finally, the characteristics of the fluids employed. More details about the CALMEC model are available in<sup>58,59</sup>.

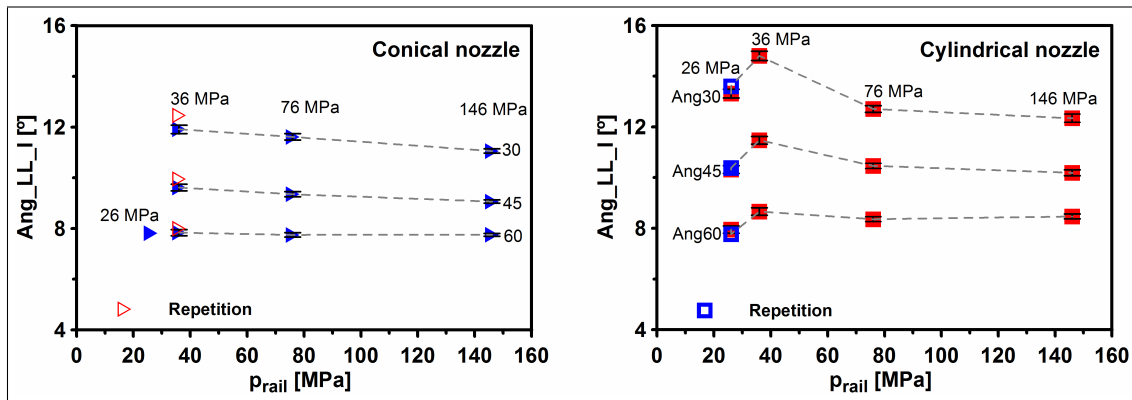


**Figure 9.** Evolution of Ang\_LL\_I (obtained from direct measurement from the spray liquid length images) versus  $p_{rail}$ . **Left.**-Conical nozzle. **Right** Cylindrical nozzle.

A single cylinder engine will be used to measure the instantaneous in-cylinder pressure. Regarding the testing methodology, several aspects can be mentioned: firstly, the operating conditions used in the engine during the tests for the conical and the cylindrical nozzles were the same (i.e. same engine speed, intake pressure and temperature, etc.). Secondly, for both nozzles and  $p_{rail}$  levels (76 and 146 MPa), a sweep of injection timings was carried out, so as to modify the relative position of the combustion process in the cycle. Thanks to this methodology, a set of tests with different CA50 (the angle where 50% of the fuel mass has been burned) is available for each nozzle and  $p_{rail}$ , thus allowing the selection of cases with identical position of the combustion process in the cycle (i.e. identical CA50) for a fairer comparison. The main reason for this choice is that in two tests with the same CA50, the piston position, in average, is the same, and therefore the in-cylinder thermodynamic conditions (temperature and air density) will be the same. Thirdly, for the two  $p_{rail}$  levels tested, the same fuel mass was injected so as to work with identical global  $F$  (Fuel/air ratio) in both cases. And, finally, long injections of around 2 ms were used to ensure diffusive (i.e. mixing controlled) combustions, since it is only under these circumstances that the spray theory can be applied, which will allow extracting information about the spray cone angle.

The evolution of the instantaneous in-cylinder pressure was recorded at each of the experiments to determine the HRF through the CALMEC model. In Figure 10 the evolution of the HRF (non-dimensional) versus crank angle for different injection timings is shown. The tests were performed with the conical nozzle and a  $p_{rail}$  level of 76 MPa.

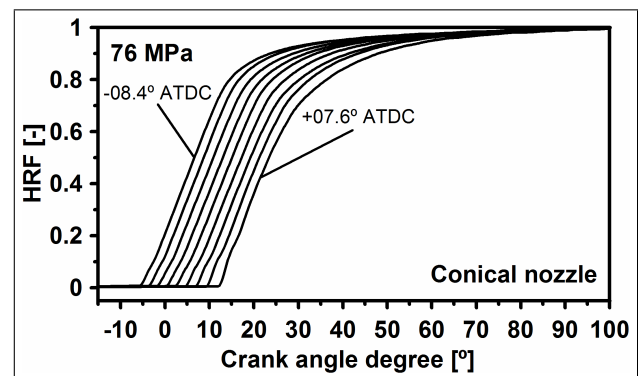


**Figure 10.** Evolution of the HRF (non-dimensional) versus crank angle, for different injection timings, for the conical nozzle and 76 MPa of  $p_{rail}$ .

The ACT parameter (*Apparent Combustion Time*)<sup>60</sup> will be used to analyze the mixing process. Since the combustion process is mixing-controlled, because of its diffusive character, the ACT, a parameter that will be explained in the following paragraphs, can be used as an indicator of the characteristic mixing time. In Figure 11, two pieces of information are shown: on the one hand, the cumulated injected fuel mass (dashed line) and, on the other hand, the burned fuel mass (continuous line), both normalized from 0

to 100% and plotted versus time. From this figure it can be seen that the ACT parameter corresponds to the (apparent) time that the injected fuel takes to burn.

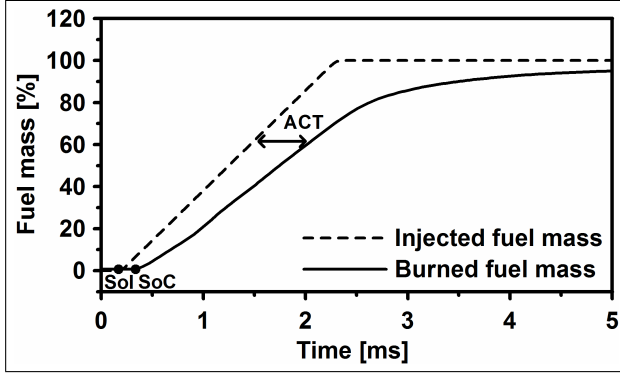


**Figure 11.** Injected and burned fuel mass versus time. This information is from the conical nozzle,  $p_{rail}$  level of 146 MPa and injection timing of  $-0.4^\circ ATDC$ . The apparent combustion time (ACT) represents a characteristic combustion time.

The evolution of the ACT parameter can be plotted for each nozzle,  $p_{rail}$  level, and injection timing as a function of the percentage of the fuel mass. This is shown in Figure 12 for different injection timings for the conical nozzle and 76 MPa of  $p_{rail}$ . In addition, a region marked with a grey square is also shown in the figure, indicating the range where an average value for the ACT parameter will be computed, which later will be used to analyze the results.

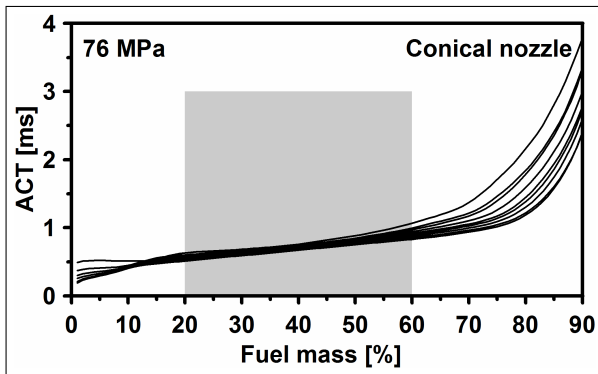


**Figure 12.** Evolution of the ACT parameter versus the percentage of the fuel mass, for different injection timings, for the conical nozzle and 76 MPa of  $p_{rail}$  level.

In Figure 13, the average ACT for each of the injection timings,  $p_{rail}$  levels (36, 76 and 146 MPa), and nozzles studied, is plotted versus CA50 (i.e. the angle giving the combustion position in the cycle). In addition, a fitting curve

for each case (nozzle and pressure) is also shown in the figure. The purpose of these fits is twofold: firstly, to filter the possible experimental uncertainties and, secondly, to allow interpolation and/or extrapolation to other values of CA50 not tested.

Now, the methodology that will be used to obtain the spray cone angle from the ACT parameter will be described.

### Obtaining the spray cone angle from the ACT parameter

Equation 10 defines the characteristic mixing time obtained by application of the spray theory<sup>61</sup>:

$$t_{mix} \propto \frac{1}{\tan(\theta/2)} \cdot d_{eff} \cdot \frac{1}{u_{eff}} \cdot \left(\frac{\rho_f}{\rho_a}\right)^{\frac{1}{2}} \quad (10)$$

where:  $t_{mix}$  is the characteristic mixing time,  $\theta$  is the spray cone angle,  $d_{eff}$  is the effective diameter,  $u_{eff}$  is the effective injection velocity, and  $\rho_a$  and  $\rho_f$  are the air and the fuel densities, respectively. It is worthy to note that  $t_{mix}$  (the characteristic mixing time) is equivalent to the ACT parameter. Therefore, Equation 10 can be rewritten in the following way:

$$ACT \equiv t_{mix} \propto \frac{1}{\tan(\theta/2)} \cdot d_{eff} \cdot \frac{1}{u_{eff}} \cdot \left(\frac{\rho_f}{\rho_a}\right)^{\frac{1}{2}} \quad (11)$$

The cases from the conical and cylindrical nozzles will be compared at iso-CA50, to ensure that the in-cylinder thermodynamic conditions (temperature and density) are the same. Taking into account this fact, Equation 11 can be simplified to the next equation:

$$ACT \equiv t_{mix} \propto \frac{1}{\tan(\theta/2)} \cdot d_{eff} \cdot \frac{1}{u_{eff}} \quad (12)$$

The term  $\tan(\theta/2)$  from Equation 12 can be isolated, leading to Equation 13:

$$\tan(\theta/2) \propto \frac{d_{eff}}{u_{eff} \cdot ACT} \quad (13)$$

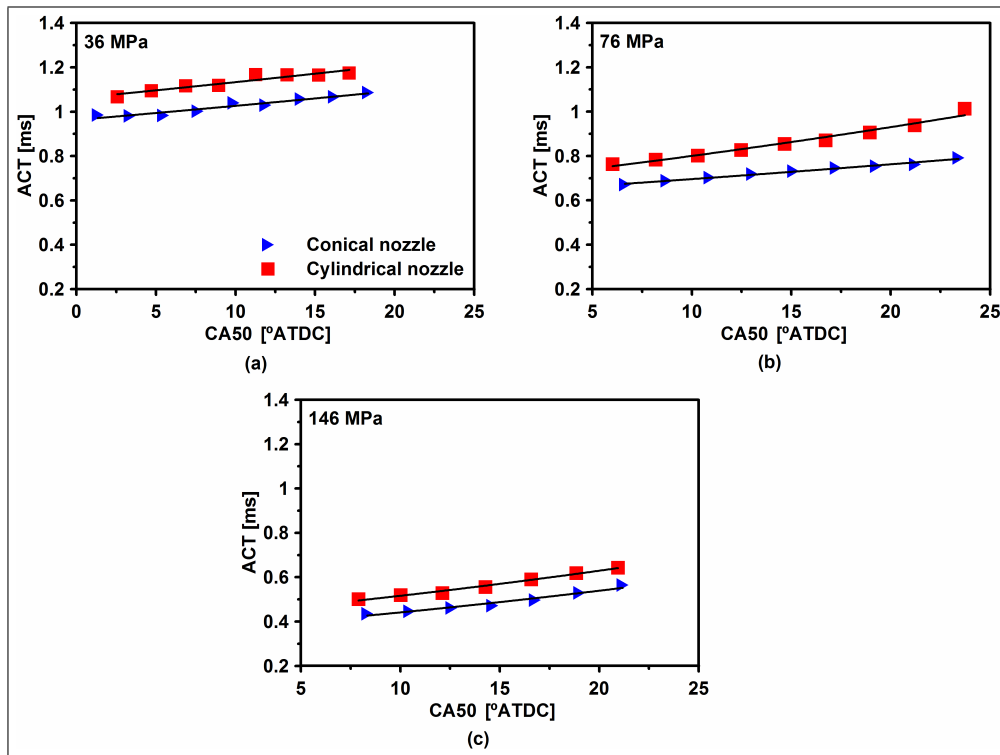


**Figure 13.** Average ACT versus CA50, for different injection timing for the conical and cylindrical nozzles, and  $p_{rail}$  levels of 36, 76 and 146 MPa.

It is important to note that the spray cone angle obtained in this way corresponds to real conditions, i.e. evaporative and reactive spray, and it will be referred as Ang\_ACT further on.

Now, the main results and the discussion of the present study will be presented.

## Results and discussion

### Effect of cavitation on the effective diameter and the effective injection velocity

In Figure 14, to the left, the evolution of  $C_v$  for the conical and cylindrical nozzles versus the root square of the cavitation number ( $\sqrt{K}$ ) is shown. In the same figure, to the right, the same information is presented but now the values of  $C_v$  have been normalized with the corresponding value of  $C_v$  from the conical nozzle (that's the reason why all the values for the conical nozzle are 1). Also in this way, the results of  $C_v$  are totally equivalent to those of  $u_{eff}$ . The cavitation number was proposed by Nurick<sup>7</sup> to quantify the cavitation level in a nozzle, and is defined in the next way:

$$K = \frac{p_{inj} - p_{vap}}{p_{inj} - p_{back}} \quad (14)$$

where  $p_{rail}$  is the rail pressure,  $p_{back}$  is the back pressure, and  $p_{vap}$  is the vapor pressure of the fuel at the temperature existing in the nozzle.

In Figure 15, the same information from Figure 14 is presented but plotted versus  $p_{rail}$ .

From the behavior of  $C_v$  for the cylindrical nozzle in Figure 14, to the right, two aspects can be seen: firstly, the  $C_v$  increases when the cavitation level increases (i.e. when the  $\sqrt{K}$  is reduced). This result is coherent with the bibliography<sup>21</sup>. Secondly, despite the increase of  $C_v$  as a consequence of cavitation, its value never reaches the one corresponding to the conical nozzle. In order to check the validity and/or the generality of this result, some other results from other studies (and, thus, from other nozzles) similar to the present one have been collected from the literature. The geometrical details of these other nozzles are given in Table 4. The reader should note that the nozzles have been

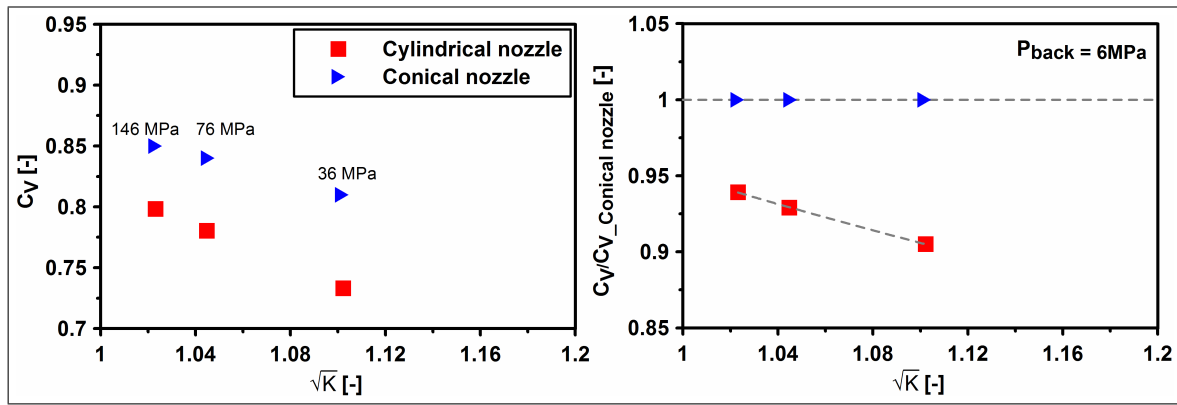


**Figure 14.** Evolution of  $C_v$  versus  $\sqrt{K}$  for the conical and cylindrical nozzles. **Left.**-Values of  $C_v$ . **Right.**-Values of  $C_v$  normalized with the corresponding value of  $C_v$  from the conical nozzle.

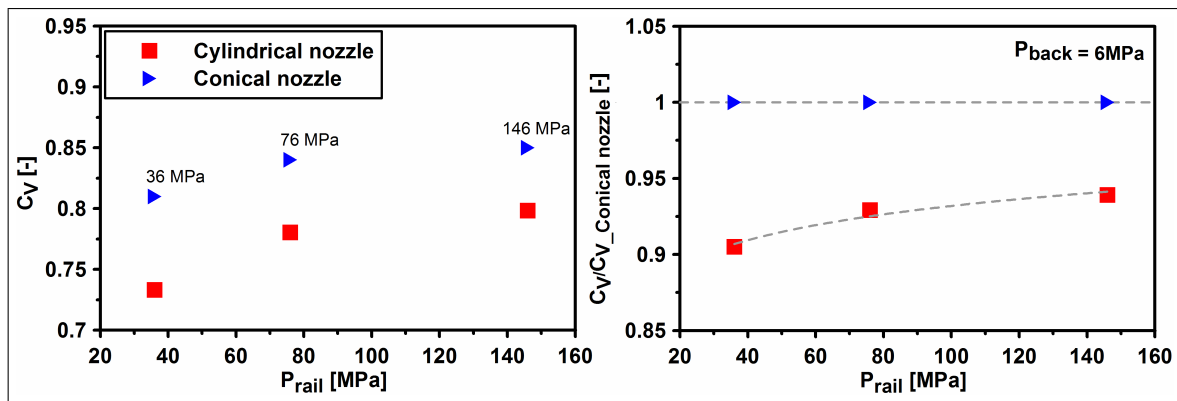


**Figure 15.** Evolution of  $C_v$  versus  $p_{rail}$  for the conical and cylindrical nozzles. **Left.**-Values of  $C_v$ . **Right.**-Values of  $C_v$  normalized with the corresponding value of  $C_v$  from the conical nozzle.

organized by couples, i.e. conical nozzle - cylindrical nozzle, since they will be analyzed in the same way as the two nozzles studied in the present work.

Now, the analysis already performed in Figure 14 will be repeated for all the couples of nozzles from Table 4. The corresponding results are shown in Figure 16, where the information corresponding to the conical and cylindrical nozzles is presented in the same format as before: the evolution of  $C_v$  versus  $\sqrt{K}$  (left) and the evolution of the normalized  $C_v$  (referred to the corresponding conical nozzle) versus  $\sqrt{K}$  (right).

In Figure 16, to the right, it is observed that the behavior of  $C_v$  for all the nozzles is coherent with the one previously observed in Figure 14. Consequently, two facts have been confirmed: on the one hand, the increase of  $C_v$  with the increase of the cavitation level and, on the other hand, the

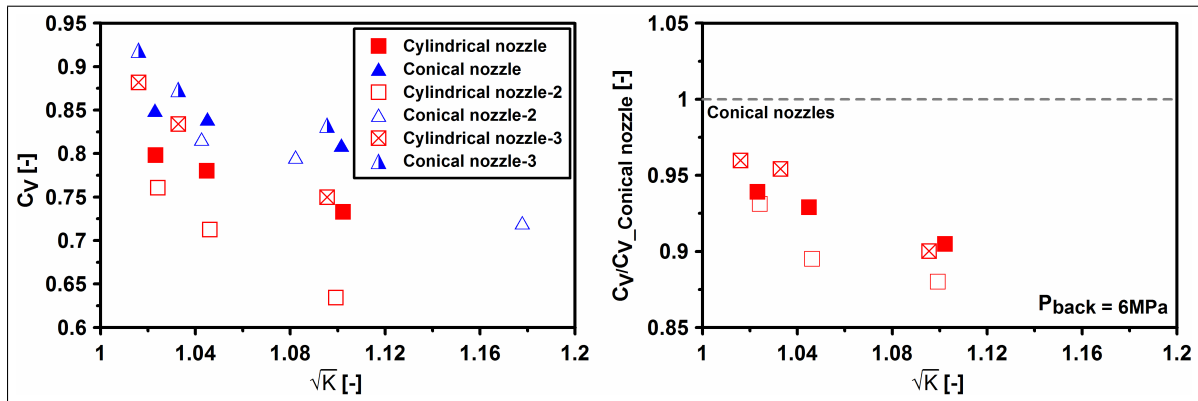
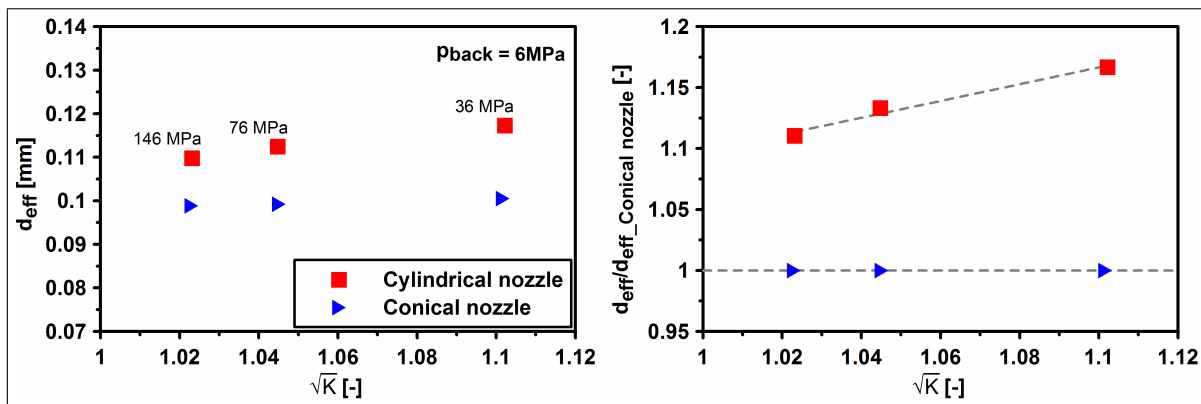
$C_v$  for the conical nozzle is higher compared to that for the cylindrical nozzle.

In Figure 17, to the left, the evolution of  $d_{eff}$  versus  $\sqrt{K}$  for the conical and cylindrical nozzles is shown. As in the previous case, in the same figure, to the right, the same information is presented but now the values of  $d_{eff}$  have been normalized with the corresponding value of  $d_{eff}$  from the conical nozzle.

If the trend of  $d_{eff}$  for the cylindrical nozzle in Figure 17, to the right, is studied, two aspects can be observed: firstly, the  $d_{eff}$  decreases with the increase of the cavitation level (i.e. when the  $\sqrt{K}$  is reduced). This result is consistent with the bibliography. And, secondly, the  $d_{eff}$  for the cylindrical nozzle is bigger compared to the one of the conical nozzle (between 11 and 17% higher). Therefore, the permeability of the cylindrical nozzle is higher compared to the one of

**Table 4.** Geometrical details of the nozzles collected from the literature.

Source of data	Nozzle Nomenclature	Type of nozzle and geometry	Sac geometry	$d_{in}$ [ $\mu m$ ]	$d_{out}$ [ $\mu m$ ]	k-factor [-]
O. A. de la Garza <sup>62</sup>	Cylindrical nozzle-2	Multi-hole cylindrical	Mini-sac	147	147	0
	Conical nozzle-2	Multi-hole conical	Mini-sac	151	138	1.7
R. Payri et al. <sup>3</sup>	Cylindrical nozzle-3	Multi-hole cylindrical	Mini-sac	175	175	0
	Conical nozzle-3	Multi-hole conical	Mini-sac	176	160	1.6

**Figure 16.** Evolution of  $C_v$  versus  $\sqrt{K}$  for the nozzles described in Tables 1 and 4. **Left.**-Values of  $C_v$ . **Right.**-Values of  $C_v$  normalized with the corresponding value of  $C_v$  from the conical nozzle.**Figure 17.** Evolution of  $d_{eff}$  versus  $\sqrt{K}$  for the conical and cylindrical nozzles. **Left.**-Values of  $d_{eff}$ . **Right.**-Values of  $d_{eff}$  normalized with the corresponding value of  $d_{eff}$  from the conical nozzle.

the conical nozzle. It is important to remark that this is a particular result of this study. In fact, when the study was defined, the two nozzles were intended to be built with the same permeability. However, based on these results, it was not finally achieved due to a manufacturing problem.

Once the behavior of the parameters  $d_{eff}$  and  $C_v$  has been studied, the effect of cavitation on the spray cone angle will be analyzed.

### Effect of cavitation on the spray cone angle

As already mentioned in the “characterization of the spray cone angle” section, the spray cone angle has been characterized in two different scenarios. The first scenario was through the analysis of the images of liquid phase (near realistic conditions, i.e. evaporative but non-reactive spray). As indicated previously, in this scenario two spray cone angles will be analyzed: on the one hand, it will be

obtained through the functional dependence of the liquid length ( $Ang_{LL,F}$ ) and, on the other hand, it will be obtained through direct measurement on the images of the liquid phase ( $Ang_{LL,I}$ ). And the second scenario was to obtain the spray cone angle through the heat release fraction, which are fully-realistic conditions, i.e. evaporative and reactive spray ( $Ang_{ACT}$ ).

#### *From the images of liquid phase*

In Figure 18, to the left, the evolution of  $Ang_{LL,F}$  versus  $p_{rail}$  for the conical and cylindrical nozzles is shown. As already done in the previous section, in the same figure, to the right, the same information is presented but now the values of  $Ang_{LL,F}$  have been normalized with the corresponding values of the conical nozzle.

Before extracting any conclusion from Figure 18, two aspects should be taken into account: firstly, as already mentioned previously, the experimental dispersion of the measurement of the liquid length for the conical and the cylindrical nozzles is very similar. And secondly, it is well-known that increasing the pressure level leads to an increase in the fuel temperature, which also affects the  $Y_{f,evap}$  and, hence the determination of the spray cone angle. However, if the spray cone angle is analyzed at iso- $p_{rail}$  (like performed here), this problem is solved.

Taking into account these aspects, in Figure 18, to the right, it can be observed that the cylindrical nozzle has a higher spray cone angle compared to the conical nozzle for the  $p_{rail}$  levels of 36, 76 and 146 MPa, which might be caused by the cavitation phenomenon. More precisely, the average percentage of increase in spray cone angle is around 3.79, 3.07 and 2.07%, respectively, for the  $p_{rail}$  levels of 36, 76 and 146 MPa.

In Figure 19, the results of  $Ang_{LL,I}$  are shown. More precisely, in the figure, to the left, the evolution of  $Ang_{LL,I}$  versus  $p_{rail}$  for the conical and cylindrical nozzles is presented. As in the previous cases, in the same figure, to the

right, the same information is presented but now the values of  $Ang_{LL,I}$  have been normalized with the corresponding case for the conical nozzle.

Before extracting any conclusion from the figure, it should be taken into account that the spray cone angle obtained from the images of the liquid phase is not the real spray cone angle (i.e. the corresponding to the whole spray, and consequently including both the liquid and the vapor phases), since only the liquid phase is visualized. However, both cone angles should keep a relationship (a proportionality factor). For this reason, the results illustrated in Figure 19 should be analyzed in a qualitative way.

In the figure, to the right, it can be seen that the cylindrical nozzle has a bigger  $Ang_{LL,I}$  compared to the conical nozzle, most probably as a consequence of the cavitation phenomenon, for the  $p_{rail}$  levels of 36, 76 and 146 MPa. However, at 26 MPa, both angles are equivalent, thus showing that there is no cavitation at these conditions, which seems reasonable. These results qualitatively show good agreement with those presented in the previous section, when the spray cone angle issued from the functional dependence of the liquid length was analyzed.

In the upcoming section, the effect of cavitation on the spray cone angle obtained from the heat release fraction will be analyzed.

#### *From the heat release fraction*

In Figure 20, to the left, the evolution of  $Ang_{ACT}$  (referred to the spray cone angle obtained from the heat release fraction) versus  $p_{rail}$  for the conical and cylindrical nozzles is shown at different CA50 (CA50=7.5°, 8.5°, 9.5°, 10.5°, 11.5°, 12.5°, 13.5° and 14.5°). As already usual in the present work, in the figure, to the right, the same information is presented but now the values of  $Ang_{ACT}$  have been normalized by the corresponding values of the conical nozzle. In this figure, it can be seen that the cylindrical nozzle shows a larger spray cone angle compared to the conical

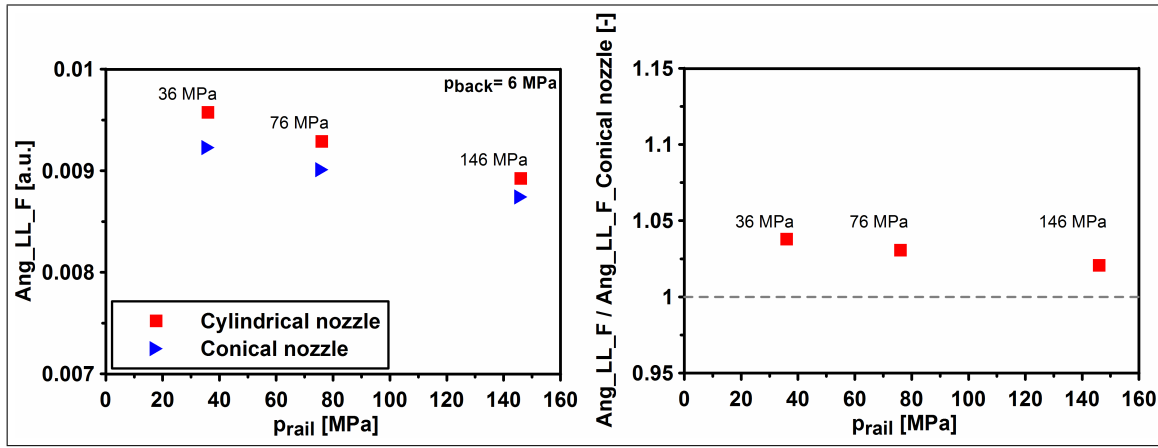


**Figure 18.** Evolution of Ang\_LL.F versus  $p_{rail}$  for the conical and cylindrical nozzles. **Left.**-Values of Ang\_LL.F. **Right.**-Values of Ang\_LL.F normalized with the corresponding value of Ang\_LL.F from the conical nozzle.

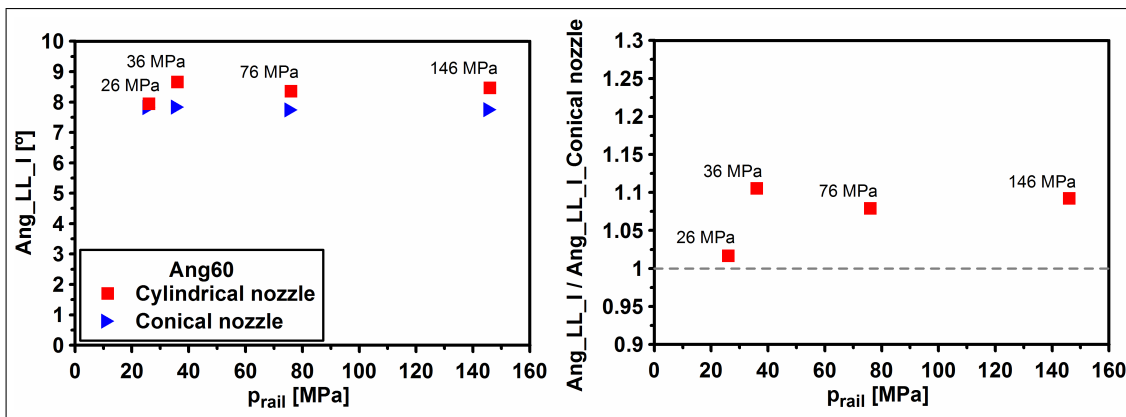


**Figure 19.** Evolution of Ang\_LL.I versus  $p_{rail}$  for the conical and cylindrical nozzles. **Left.**-Values of Ang\_LL.I. **Right.**-Values of Ang\_LL.I normalized with the corresponding value of Ang\_LL.I from the conical nozzle.

nozzle as a consequence of the cavitation phenomenon. More specifically, the average percentage of increase in spray cone angle for the cases at CA50=11.5° (the average value of all the CA50 cases shown in the figure), is around 5.0 and 3.6%, respectively, for the cases with a  $p_{rail}$  of 76 and 146 MPa.

In Figure 21, the results shown in Figures 18 and 20 are synthesized. Specifically, the evolution of the normalized Ang\_LL.F versus the normalized Ang\_ACT for the cylindrical nozzle for different cases at iso-CA50 is presented. From this figure, two aspects can be mentioned: (1) the results obtained from the functional dependence of the liquid length qualitatively show good agreement with those obtained from the heat release fraction (a bisecting line has been included in the plot as an indication of a perfect match between the two angle definitions), and (2) the

quantitative difference between these results was expected, since now experiments have been carried out in fully-realistic conditions (i.e. evaporative and reactive spray).

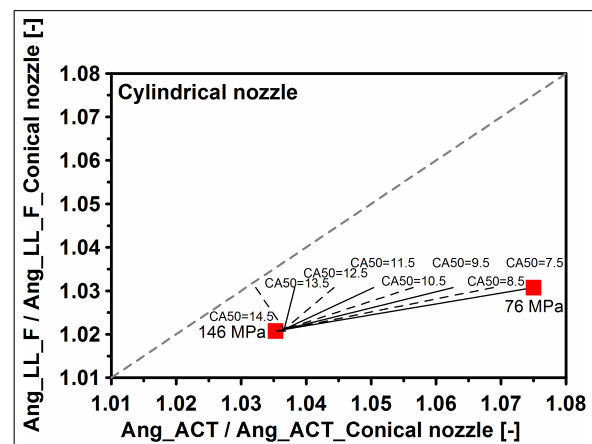


**Figure 21.** Evolution of Ang\_LL.F versus Ang\_ACT for the cylindrical nozzle for different cases at iso-CA50. The values have been normalized with the corresponding one for the conical nozzle.

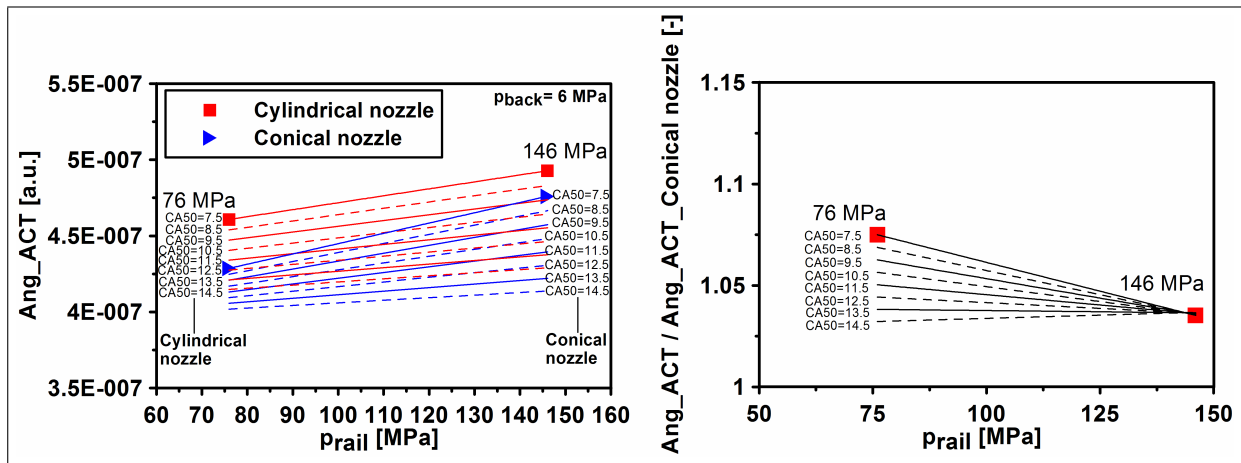


**Figure 20.** Evolution of Ang\_ACT versus  $p_{rail}$  for the conical and cylindrical nozzles for different cases to iso-CA50. **Left.**-Values of Ang\_ACT. **Right.**-Values of Ang\_ACT normalized with the corresponding value of Ang\_ACT from the conical nozzle.

A final remark is that, even through this procedure to calculate the spray cone angle is, by far, more complex compared to the procedure used in the previous section, it is obtained in fully realistic conditions and involves less inaccuracies than the other method, and the values obtained for this case are more or less an average value of all the values obtained with the different methods. Therefore this last results (from the heat release fraction) will be chosen to be used in the final analysis.

In the next section a synthesis of the results obtained about the mixing process in the two different scenarios (i.e. non-reacting and reacting) will be carried out.

#### *Synthesis of the results obtained about spray cone angle*

In Table 5, a comparison of the different increments in spray cone angle obtained in the previous sections is shown: (a) from the liquid length and applying its functional dependence (Ang\_LL\_F), (b) from a direct measurement from the images of the liquid phase (Ang\_LL\_I) and, (c) from the heat release fraction (Ang\_ACT), in all cases for the  $p_{rail}$  levels of 76 and 146 MPa.

From this table, two conclusions can be extracted: on the one hand, that the results obtained about the spray cone angle are all qualitatively consistent and, on the other hand, that there are significant differences (quantitatively speaking) between the values obtained from the different methods.

These quantitative differences between the two analyzed scenarios, as mentioned previously, were already expected because of two reasons: firstly, because the conditions used in each of the scenarios were different (in one of the scenarios, an evaporative but non-reacting spray was analyzed, while in the other, an evaporative and reacting spray was considered). And, secondly, because of the significant differences in the procedure used at each scenario to determine the spray cone angle.

Now an effort will be done to try to link two of the conclusions previously described in this work: on the one hand, that the  $u_{eff}$  from the cylindrical nozzle increases with the increase of the cavitation level, but never reaching the  $u_{eff}$  from the conical nozzle and, on the other hand, that the spray cone angle of the cylindrical nozzle is higher compared to the conical nozzle, also as a consequence of cavitation. From these two observations, it can be stated that the wider spray cone angle at the cylindrical nozzle is not due to an increase in  $u_{eff}$ , but most probably to the biphasic flow inside the nozzle hole. This statement is consistent with the conclusion achieved by several authors, as for instance Kent and Brown<sup>63</sup>, and Chehroudi et al.<sup>64</sup>, who concluded that the injection pressure, which is closely related to the  $u_{eff}$ , has an effect practically negligible on the spray cone angle.

**Table 5.** Comparison of the increase in spray cone angle, obtained from the liquid length (cases a and b) and from the heat release fraction (case c) .

$P_{rail}$ [MPa]	Increase of spray cone angle [%] (a)	Increase of spray cone angle [%] (b)	Increase of spray cone angle [%] (c)
76	3.0	7.9	5.0
146	2.0	9.2	3.6

In summary, the cylindrical nozzle compared to the conical nozzle and for the  $p_{rail}$  levels of 76 MPa (medium level of cavitation) and 146 MPa (high level of cavitation) presents, on the one hand, a  $u_{eff}$  lower of around 7.0% and 6.0%, respectively for the  $p_{rail}$  levels of 76 and 146 MPa. And, on the other hand, an increase in spray cone angle (Ang\_ACT) of around 5.0% and 3.6%, respectively. It is worthy to point out that these last results correspond to the second scenario employed for the characterization of the spray cone angle, i.e. from the heat release fraction, since it is obtained in fully realistic conditions and involves less inaccuracies than the other method, and the values obtained for this case are more or less an average value of all the values obtained with the different methods.

Once this point reached, a question arises: which parameter does have more influence on the mixing process, the variation of  $u_{eff}$  or the variation of the spray cone angle, both as a consequence of cavitation? To give an answer to this question, the influence of the variations of  $u_{eff}$  and the spray cone angle on the ACT parameter (Apparent Combustion Time) for  $p_{rail}$  levels of 76 and 146 MPa for the cylindrical and the conical nozzles will be analyzed. To do so, the following expression of the ACT parameter, derived from Equation 13, will be used:

$$ACT \propto \left( \frac{1}{u_{eff} \cdot \tan(\theta/2)} \right) \quad (15)$$

From Equation 15 and taking into account the results obtained during the comparison of the cylindrical with the conical nozzle, it can be said:

- At the  $p_{rail}$  level of 76 MPa, a reduction in  $u_{eff}$  ( $C_v$ ) of a factor of 0.929, i.e. 7.1%, and an increase in spray

cone angle of a factor of 1.05, i.e. 5%. The combined influence on the mixing time (i.e. the ACT parameter) is an increase in a factor of 1.025, i.e. 2.5%.

- At the  $p_{rail}$  level of 146 MPa, a reduction in  $u_{eff}$  ( $C_v$ ) of a factor 0.939, i.e. 6.1%, and an increase in spray cone angle of a factor of 1.036, i.e. 3.6%. The combined influence on the mixing time is an increase in a factor of 1.028, i.e. 2.8%.

Therefore, analyzing on a whole the variation of  $u_{eff}$  and the spray cone angle when comparing the cylindrical nozzle with the conical one, for the cases studied here, it is found that the mixing process worsens with the cylindrical nozzle.

## Conclusions

This work has intended to deepen the knowledge about the influence of cavitation on the mixing process in diesel nozzles through the study of the influence of cavitation on the effective diameter, the effective injection velocity and the spray cone angle, parameters that affect the mixing process. The spray cone angle was studied in two different scenarios. The first scenario was based on images of the liquid phase (nearly realistic conditions, i.e. evaporative but non-reactive spray). In this scenario two spray cone angles were analyzed: on the one hand, the spray cone angle obtained through the functional dependence of the liquid length and, on the other hand, the spray cone angle obtained through the direct measurement from the images of the liquid phase. The second scenario, however, was based on the heat release fraction (fully-realistic conditions, i.e. evaporative and reactive spray). It is worthy to indicate that the studies available in the literature related to characterization of the

spray cone angle in fully-realistic conditions, i.e. evaporative and reactive spray are very scarce. Now the main conclusions of the study will be summarized.

Regarding the effective diameter and the effective injection velocity, for the cylindrical nozzle, the reduction in the effective diameter and the increase in the effective injection velocity, both as a consequence of cavitation, were confirmed. However, despite the increase in  $u_{eff}$ , this parameter never reaches the corresponding value of the conical nozzle. Based on the information collected from the literature, this statement is consistent.

Concerning the spray cone angle, the increase in spray cone angle as a consequence of cavitation has been confirmed in both analyzed scenarios, even if there is a significant difference in the values obtained of around 4% between the two. This difference, however, was already expected because of the following two main reasons: firstly, because the conditions used in each of the scenarios were different (in the first scenario an evaporative but non-reactive spray was analyzed, whereas in the other an evaporative and reactive spray was studied). And, secondly, because of the significant differences in the procedure used to determine the spray cone angle at each scenario.

The increase in spray cone angle caused by cavitation can not be due to an increase in  $u_{eff}$ , since it is lower for the cavitating nozzle. The explanation of this increase in spray cone angle might be the biphasic flow inside the nozzle hole. However, the validation of this hypothesis will require additional research, and it is out of the scope of the present publication.

The reduction of the effective diameter, the increase of the effective injection velocity, and the increase of the spray cone angle, all of them as a consequence of cavitation, lead to a better mixing process respect to the case with no cavitation when working with a given nozzle. However, if the mixing process between the two nozzles is compared, for the cases studied here, it worsens with the cylindrical nozzle

despite the benefits associated to the cavitation phenomenon mentioned previously.

## Acknowledgements

The authors would like to thank Gabriel Alcantarilla, who is a member of the CMT-Motores Térmicos team, for his support in carrying out the experimental measurements in the single-cylinder engine. Also to José María Bordes for his contribution to the work.

## Funding

The authors would like to thank the FPU program of the Spanish Ministry of Education is greatly acknowledged for supporting the PhD studies of Oscar A. de la Garza (grant: AP2008-01913). Finally, many thanks to PSA Peugeot-Citroën, National Council of Science and Technology (CONACYT) of the Mexican Government (project: CB-239943) and the Royal Academy of Engineering, United Kingdom (project: NRCP/1415/238) for supporting this research.

## Declaration of conflicting interest

The Authors declare that there are no conflicts of interest.

## Notation

$ACT$	Apparent Combustion Time
$A$	Area
$Ang30$	Angle obtained considering only the spray contour up to 30% of the spray tip penetration
$Ang45$	Angle obtained considering only the spray contour up to 45% of the spray tip penetration
$Ang60$	Angle obtained considering only the spray

	contour up to 60% of the spray		
	tip penetration		
<i>Ang_LL_F</i>	Spray cone angle obtained from the functional dependence of the liquid length		
<i>Ang_LL_I</i>	Spray cone angle obtained from direct measurement it with the images of liquid phase		
<i>Ang_ACT</i>	Spray cone angle obtained from the heat release fraction		
<i>C<sub>d</sub></i>	Discharge coefficient		
<i>C<sub>M</sub></i>	Momentum coefficient		
<i>C<sub>a</sub></i>	Area coefficient		
<i>C<sub>v</sub></i>	Velocity coefficient		
<i>CA50</i>	Angle where 50% of the fuel mass has been burned		
<i>d</i>	Diameter		
<i>F</i>	Fuel/air ratio		
<i>HRF</i>	Heat Release Fraction		
<i>K</i>	Cavitation number from Nurick ( $\frac{p_{inj} - p_{vap}}{p_{inj} - p_{back}}$ )		
<i>LL</i>	Liquid length		
<i><math>\dot{m}</math></i>	Mass Flow Rate		
<i><math>\dot{M}</math></i>	Momentum Flux		
<i>p</i>	Pressure		
<i>SoC</i>	Start of Combustion		
<i>SoI</i>	Start of Injection		
<i>s</i>	Spray penetration		
<i>t</i>	Time		
<i>u</i>	Velocity		
<i>VCO</i>	Valve Covered Orifice		
<i>Y</i>	Mass fraction		

### Greek symbols

$\Delta$	Increase
$\theta$	Spray cone angle
$\rho$	Density
$\sigma$	Standard deviation

### Subscripts

<i>a</i>	Referred to air
<i>back</i>	Referred to the volume where the fuel is injected
<i>cyl</i>	Referred to cylinder
<i>eff</i>	Effective
<i>f, evap</i>	Referred to evaporation of fuel
<i>f</i>	Referred to fuel
<i>in</i>	At the inlet of the nozzle hole
<i>inj</i>	Referred to injection pressure
<i>mix</i>	Referred to mixing
<i>out</i>	At the outlet of the nozzle hole
<i>rail</i>	Referred to common rail
<i>th</i>	Referred to Bernoulli (theoretical)
<i>vap</i>	Referred to fuel vapor

### References

1. Karra PK, Kong SC. Experimental study on effects of nozzle hole geometry on achieving low diesel engine emissions. *J Eng Gas Turbine Power*. 2009;132:022802–10.
2. Som S, Ramirez AI, Longman DE, Aggarwal S. Effect of nozzle orifice geometry on spray, combustion, and emission characteristics under diesel engine conditions. *Fuel*. 2011;90:1267–1276.
3. Payri R, Salvador FJ, Gimeno J, Zapata LD. Diesel nozzle geometry influence on spray liquid-phase fuel penetration in evaporative conditions. *Fuel*. 2008;87:1165–1176.

4. Wang X, Huang Z, Zhang W, Kuti OA, Nishida K. Effects of ultra injection pressure and micro-hole nozzle on flame structure and soot formation of impinging diesel spray. *Applied Energy*. 2011;88:1620–1628.
5. Watanabe H, Nishikori M, Hayashi T, Suzuki M, Kakehashi N, Ikemoto M. Visualization analysis of relationship between vortex flow and cavitation behavior in diesel nozzle. *International Journal of Engine Research*. 2015;16:5–12.
6. Hayashi T, Suzuki M, Ikemoto M. Effects of internal flow in a diesel nozzle on spray combustion. *International Journal of Engine Research*. 2013;14:646–653.
7. Nurick WH. Orifice cavitation and its effects on spray mixing. *Journal of fluids engineering*. 1976;98:681–687.
8. Schmidt DP, Rutland CJ, Corradini ML. A numerical study of cavitating flow through various nozzle shapes; 1997. SAE Paper 971597.
9. Payri F, López JJ, García A, de la Garza OA, Houille S. Effects of cavitation in common-rail diesel nozzles on the soot formation process; 2013. SAE Paper 2013-01-1602.
10. Gavaises M, Andriotis A, Papoulias D, Mitroglou N, Theodorakakos A. Characterization of string cavitation in large-scale Diesel nozzles with tapered holes. *Physics of Fluids*. 2009;21(5):052107.
11. Reid BA, Hargrave GK, Garner CP, Wigley G. An investigation of string cavitation in a true-scale fuel injector flow geometry at high pressure. *Physics of Fluids*. 2010;22.
12. Mitroglou N, Gavaises M. Mapping of cavitating flow regimes in injectors for medium-/heavy-duty diesel engines. *International Journal of Engine Research*. 2013;14(6):590–605.
13. Mitroglou N, McLorn M, Gavaises M, Soteriou C, Winterbourne M. Instantaneous and ensemble average cavitation structures in Diesel micro-channel flow orifices. *Fuel*. 2014;116:736–742.
14. Desantes JM, Salvador FJ, Carreres M, Martínez-López J. Large-eddy simulation analysis of the influence of the needle lift on the cavitation in diesel injector nozzles. *Proceedings of the Institution of Mechanical Engineers, Part D: Journal of Automobile Engineering*. 2014;229(4):407–423.
15. Soteriou C, Andrews R, Smith M. Direct injection diesel spray and the effect of cavitation and hydraulic flip on atomization; 1995. SAE Paper 950080.
16. Chaves H, Knapp M, Kubizek A. Experimental study of cavitation in the nozzle hole of diesel injectors using transparent nozzles; 1995. SAE Paper 950290.
17. Arcoumanis C, Flora H, Gavaises M, Badami M. Cavitation in Real-Size Multi-Hole Diesel Injector Nozzles; 2000. SAE Paper 2000-01-1249.
18. Winklhofer E, Kull E, Kelz E, Morozov A. Comprehensive hydraulic and flow field documentation in model throttle experiments under cavitation conditions; 2001. ILASS-Europe, Zurich.
19. Payri R, Salvador FJ, Gimeno J, de la Morena J. Study of cavitation phenomena based on a technique in a liquid pressurized chamber. *International Journal of Heat and Fluid Flow*. 2009;30:768–777.
20. Payri R, Salvador FJ, Gimeno J, Venegas O. Study of cavitation phenomenon using different fuels in a transparent nozzle by hydraulic characterization and visualization. *Experimental Thermal and Fluid Science*. 2013;44:235–244.
21. López JJ, Salvador FJ, de la Garza OA, Arrègle J. A comprehensive study on the effect of cavitation on injection velocity in a diesel nozzle. *Energy Conversion and Management*. 2012;64:415–423.
22. Mishra C, Peles Y. Flow visualization of cavitating flows through a rectangular slot micro-orifice ingrained in a microchannel. *Physics of Fluids*. 2005;17(11):113602.
23. Aleiferis PG, Serras-Pereira J, Augoye A, Davies TJ, Cracknell RF, Richardson D. Effect of fuel temperature on in-nozzle cavitation and spray formation of liquid hydrocarbons and alcohols from a real-size optical injector for direct-injection spark-ignition engines. *International Journal of Heat and Mass Transfer*. 2010;53(21-22):4588–4606.

24. Jiang G, Zhang Y, Wen H, Xiao G. Study of the generated density of cavitation inside diesel nozzle using different fuels and nozzles. *Energy Conversion and Management*. 2015;103:208–217.
25. Sou A, Pratama RH. Effects of Asymmetric Inflow on Cavitation in Fuel Injector and Discharged Liquid Jet. *Atomization and Sprays*. 2016;26(9):939–959.
26. Duke DJ, Swantek AB, Tilocco Z, Kastengren AL, Fezzaa K, Neroorkar K, et al. X-ray Imaging of Cavitation in Diesel Injectors; 2014. SAE Paper 2014-01-1404.
27. Yuan W, Schnerr GH. Numerical simulation of two-phase flow in injection nozzles: Interaction of cavitation and external jet formation. *Journal of Fluids Engineering*. 2003;125(6):963–969.
28. Alajbegovic A, Meister G, Greif D, Basara B. Three phase cavitating flows in high-pressure swirl injectors. *Experimental Thermal and Fluid Science*. 2002;26:677–681.
29. Som S, Longman DE, Ramírez AI, Aggarwal SK. A comparison of injector flow and spray characteristics of biodiesel with petrodiesel. *Fuel*. 2010;89:4014–4024.
30. Peng Kärholm F. Numerical modelling of diesel spray injection, turbulence interaction and combustion. PhD Thesis Chalmers University of Technology; 2008.
31. Habchi C, Dumont N, Simonin O, Soteriou C, Torres N, Andrews R. Multidimensional simulation of cavitating flows in diesel injectors by a homogeneous mixture modeling approach. *Atomization and Sprays*. 2008;18:129–162.
32. De la Morena J, Neroorkar K, Plazas AH, Peterson RC, Schmidt DP. Numerical analysis of the influence of diesel nozzle design on internal flow characteristics for 2-valve diesel engine application. *Atomization and Sprays*. 2013;23(2):97–118.
33. Brusiani F, Falfari S, Pelloni P. Influence of the diesel injector hole geometry on the flow conditions emerging from the nozzle. *Energy Procedia*. 2014;45:749–758.
34. Mohan B, Yang W, Chou SK. Cavitation in Injector Nozzle Holes - A Parametric Study. *Engineering Applications of Computational Fluid Mechanics*. 2014;8(1):70–81.
35. Molina S, Salvador FJ, Carreres M, Jaramillo D. A computational investigation on the influence of the use of elliptical orifices on the inner nozzle flow and cavitation development in diesel injector nozzles. *Energy Conversion and Management*. 2014;79:114–127.
36. Battistoni M, Xue Q, Som S, Pomraning E. Effect of Off-Axis Needle Motion on Internal Nozzle and Near Exit Flow in a Multi-Hole Diesel Injector. *SAE International Journal of Fuels and Lubricants*. 2014;7(1):2014–01–1426.
37. Xue Q, Battistoni M, Powell CF, Longman DE, Quan S, Pomraning E, et al. An Eulerian CFD model and X-ray radiography for coupled nozzle flow and spray in internal combustion engines. *International Journal of Multiphase Flow*. 2015;70:77–88.
38. Suh HK, Lee CS. Effect of cavitation in nozzle orifice on the diesel fuel atomization characteristics. *International Journal Heat Fluid Flow*. 2008;29:1001–1009.
39. Payri R, Molina S, Salvador FJ, Gimeno J. A study of the relation between nozzle geometry, internal flow and sprays characteristics in diesel fuel injection systems. *KSME International Journal*. 2004;18:1222–1235.
40. Andriotis A, Gavaises M. Influence of vortex flow and cavitation on near-nozzle diesel spray dispersion angle. *Atomization and Sprays*. 2009;19(3):247–261.
41. Bogavarapu P, Ravikrishna RV. A comparison of diesel and jatropha methyl ester (JME) spray characteristics: effect of nozzle entry radius. *Atomization and Sprays*. 2016;26(10):961–982.
42. Payri F, Arrègle J, López JJ, Hermens S. Effect of cavitation on the nozzle outlet flow, spray and flame formation in a Diesel Engine; 2006. SAE Paper 2006-01-1391.
43. Westlye FR, Battistoni M, Skeen SA, Manin J, Pickett LM, Ivarsson A. Penetration and combustion characterization of cavitating and non-cavitating fuel injectors under diesel engine conditions; 2016. SAE Paper 2016-01-0860.

44. Benajes J, Molina S, González C, Donde R. The role of nozzle convergence in diesel combustion. *Fuel*. 2008;87:1849–1858.
45. Macian V, Bermúdez V, Payri R, Gimeno J. New technique for determination of internal geometry of diesel nozzle with the use of silicone methodology. *Experimental Techniques*. 2003;27:39–43.
46. Desantes JM, Arrègle J, López JJ, Hermens S. Experimental characterization of outlet flow for different diesel nozzle geometries; 2005. SAE Paper 2005-01-2120.
47. Payri R, García JM, Salvador FJ, Gimeno J. Using spray momentum flux measurement to understand the influence of diesel nozzle geometry on spray characteristics. *Fuel*. 2005;84:551–561.
48. Bosch W. The fuel rate indicator: A new instrument for display of the characteristics of individual injection; 1966. SAE Paper 660749.
49. Bermúdez V, García JM, Juliá E, Martínez S. Engine with optically accesible cylinder head: a research tool for injection and combustion process; 2003. SAE Paper 2003-01-1110.
50. Pastor JV, Payri R, García-Olivier JM, Briceño FJ. Analysis of transient liquid and vapor phase penetration for diesel sprays under variable injection conditions. *Atomization and Sprays*. 2011;21:503–520.
51. Pastor JV, Arrègle J, Palomares A. Diesel spray images segmentation using a likelihood ratio test. *Applied Optics*. 2001;40:2876–2885.
52. García JM. Contribution to the study of turbulent combustion of DI diesel engine sprays (in Spanish). PhD Thesis Universitat Politècnica de València; 2004.
53. Siebers DL. Liquid-phase fuel penetration in diesel sprays; 1998. SAE Paper 980809.
54. Desantes JM, López JJ, García JM, Pastor JM. Evaporative diesel spray modeling. *Atomization and Sprays*. 2007;17:193–231.
55. Naber JD, Siebers DL. Effects of gas density and vaporization on penetration and dispersion of diesel sprays; 1996. SAE Paper 960034.
56. Desantes JM, Pastor JV, Payri R, Pastor JM. Experimental characterization of internal nozzle flow and diesel spray behavior. Part II: Evaporative conditions. *Atomization and Sprays*. 2005;15:517–543.
57. Delacourt E, Desmet B, Besson B. Characterization of very high pressure diesel sprays using digital imaging techniques. *Fuel*. 2005;84:859–867.
58. Lapuerta M, Armas O, Hernandez J. Diagnostic of DI diesel combustion from in-cylinder pressure signal by estimation of mean thermodynamic properties of the gas. *Applied Thermal Engineering*. 1999;19:513–529.
59. Lapuerta M, Armas O, Bermúdez V. Sensitivity of diesel engine thermodynamic cycle calculation to measurement errors and estimated parameters. *Applied Thermal Engineering*. 2000;20:843–861.
60. Arrègle J, López JJ, García JM, Fenollosa C. Development of zero-dimensional diesel combustion model. Part I: Analysis of the quasi-steady diffusion combustion phase. *Applied Thermal Engineering*. 2003;23:1301–1317.
61. Desantes JM, Arrègle J, López JJ, Cronhjort A. Scaling laws for free turbulent gas jets and diesel-like sprays. *Atomization and Sprays*. 2006;16:443–473.
62. De la Garza OA. Study on the effects of cavitation in diesel injection nozzles on the injection and soot formation processes (in Spanish). Barcelona: Editorial Reverté, S.A.; 2015.
63. Kent JC, Brown GM. Nozzle exit flow, characteristics for square-edged and rounded inlet geometries. *Combustion Science and Technology*. 1983;30:121–132.
64. Chehroudi B, Chen S, Bracco F, Onuma Y. On the intact core of full-cone sprays; 1985. SAE Paper 850126.